

# The two-photon exchange experiment at DESY

---

Alarcon, R.; Beck, R.; Bernauer, J. C.; Broering, M.; Christopher, A.; Cline, E. W.; Dhital, S.; Dongwi, B.; Fernando, I.; Finger, M.; ...

Source / Izvornik: **The European Physical Journal A, 2024, 60**

**Journal article, Published version**

**Rad u časopisu, Objavljena verzija rada (izdavačev PDF)**

<https://doi.org/10.1140/epja/s10050-024-01299-2>

Permanent link / Trajna poveznica: <https://um.nsk.hr/um:nbn:hr:217:863759>

Rights / Prava: [Attribution 4.0 International](#) / [Imenovanje 4.0 međunarodna](#)

Download date / Datum preuzimanja: **2024-10-03**



Repository / Repozitorij:

[Repository of the Faculty of Science - University of Zagreb](#)





# The two-photon exchange experiment at DESY

R. Alarcon<sup>1</sup>, R. Beck<sup>2</sup>, J. C. Bernauer<sup>3,4</sup>, M. Broering<sup>5</sup>, A. Christopher<sup>6</sup>, E. W. Cline<sup>3,5,a</sup>, S. Dhital<sup>6</sup>, B. Dongwi<sup>6</sup>, I. Fernando<sup>6</sup>, M. Finger<sup>7</sup>, M. Finger Jr.<sup>7</sup>, I. Frišić<sup>8</sup>, T. Gautam<sup>6</sup>, G. N. Grauvogel<sup>9</sup>, D. K. Hasell<sup>5</sup>, O. Hen<sup>5</sup>, T. Horn<sup>10</sup>, E. Ihloff<sup>5</sup>, R. Johnston<sup>5</sup>, J. Kelsey<sup>5</sup>, M. Kohl<sup>6</sup>, T. Kutz<sup>5,9</sup>, I. Lavrukhin<sup>11,b</sup>, S. Lee<sup>5</sup>, W. Lorenzon<sup>11</sup>, S. Lunkenheimer<sup>11</sup>, F. Maas<sup>12</sup>, R. G. Milner<sup>5</sup>, P. Moran<sup>5</sup>, J. Nazeer<sup>6</sup>, T. Patel<sup>6</sup>, M. Rathnayake<sup>6</sup>, R. Raymond<sup>11</sup>, R. P. Redwine<sup>5</sup>, A. Schmidt<sup>9</sup>, U. Schneekloth<sup>13</sup>, D. Sokhan<sup>14</sup>, M. Suresh<sup>6</sup>, C. Vidal<sup>5</sup>, Z. Yang<sup>11</sup>

- <sup>1</sup> Department of Physics and Astronomy, Arizona State University, Tempe, AZ, USA  
<sup>2</sup> Department of Physics and Astronomy, Friedrich Wilhelms Universität, Bonn, Germany  
<sup>3</sup> Center for Frontiers in Nuclear Science, Stony Brook University, Stony Brook, NY, USA  
<sup>4</sup> Riken BNL Research Center, Brookhaven National Laboratory, Upton, NY, USA  
<sup>5</sup> Laboratory for Nuclear Science, Massachusetts Institute of Technology, Cambridge, MA, USA  
<sup>6</sup> Department of Physics and Astronomy, Hampton University, Hampton, VA, USA  
<sup>7</sup> Department of Low Temperature Physics, Charles University, Prague, Czech Republic  
<sup>8</sup> Department of Physics, Faculty of Science, University of Zagreb, Zagreb, Croatia  
<sup>9</sup> Department of Physics, The George Washington University, Washington, DC, USA  
<sup>10</sup> Department of Physics, Catholic University of America, Washington, DC, USA  
<sup>11</sup> Randall Laboratory of Physics, University of Michigan, Ann Arbor, MI, USA  
<sup>12</sup> Institute of Nuclear Physics, Johannes Gutenberg Universität, Mainz, Germany  
<sup>13</sup> Deutsches Elektronen-Synchrotron DESY, Hamburg, Germany  
<sup>14</sup> Department of Physics and Astronomy, University of Glasgow, Glasgow, Scotland

Received: 10 August 2023 / Accepted: 13 March 2024 / Published online: 5 April 2024

© The Author(s) 2024

Communicated by Klaus Blaum

**Abstract** We propose a new measurement of the ratio of positron-proton to electron-proton elastic scattering at DESY. The purpose is to determine the contributions beyond single-photon exchange, which are essential for the Quantum Electrodynamics (QED) description of the most fundamental process in hadronic physics. By utilizing a 20 cm long liquid hydrogen target in conjunction with the extracted beam from the DESY synchrotron, we can achieve an average luminosity of  $2.12 \times 10^{35} \text{ cm}^{-2} \cdot \text{s}^{-1}$  ( $\approx 200$  times the luminosity achieved by OLYMPUS). The proposed two-photon exchange experiment (TPEX) entails a commissioning run at a beam energy of 2 GeV, followed by measurements at 3 GeV, thereby providing new data up to  $Q^2 = 4.6 (\text{GeV}/c)^2$  (twice the range of current measurements). We present and discuss the proposed experimental setup, run plan, and expectations.

## 1 Introduction

Elastic lepton-proton scattering is a fundamental process that allows us to study the structure of the proton. It is described

theoretically in the Standard Model by a perturbative expansion in  $\alpha \approx \frac{1}{137}$  with terms beyond leading order commonly called radiative corrections. Calculating such radiative corrections have been extensively described in the paper by Mo and Tsai [1], which also stressed the importance of electron-proton and positron-proton elastic scattering experiments, and subsequent work by Maximon and Tjon [2], and others.

In the Born or single photon exchange approximation the elastic  $e^\pm p$  scattering cross section is given by the reduced Rosenbluth cross section,

$$\frac{d\sigma_{e^\pm p}}{d\Omega} = \frac{d\sigma}{d\Omega_{Mott}} \frac{\tau G_M^{p,2} + \epsilon G_E^{p,2}}{\epsilon(1 + \tau)}, \quad (1)$$

where  $\tau = \frac{Q^2}{4M_p^2}$  and  $\epsilon = (1 + 2(1 + \tau) \tan^2 \frac{\theta_l}{2})^{-1}$ .

Measurements using the unpolarized Rosenbluth separation technique yielded values for  $G_E^p$  and  $G_M^p$ . Their ratio,  $\mu^p G_E^p / G_M^p$ , was found to be close to unity over a broad range in  $Q^2$  (shown by the blue data points in Fig. 1) leading to the proton form factors being envisaged as very similar and often modeled by the same dipole form factor.

However, recent measurements using polarization techniques revealed a completely different picture with the ratio

<sup>a</sup> e-mail: ewcline@mit.edu (corresponding author)

<sup>b</sup> e-mail: ievgen@umich.edu (corresponding author)

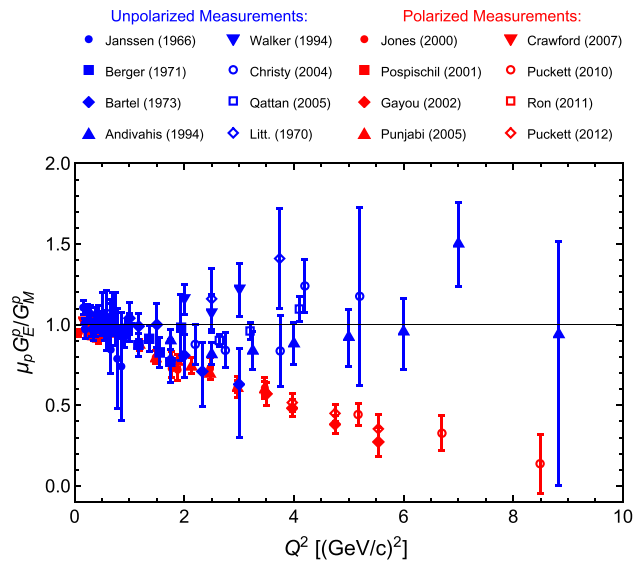


**Fig. 1** Proton form factor ratio measured using unpolarized [3–10] (blue) and polarized [11–18] (red) techniques

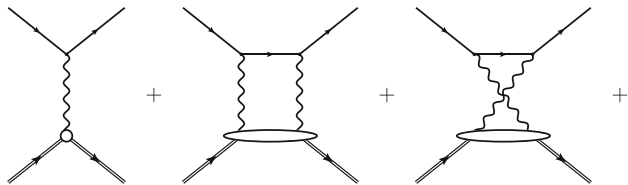


**Fig. 2** Feynman diagrams for one- and two-photon exchange. Further diagrams for bremsstrahlung, vertex, self-energy, and vacuum polarization radiative corrections are not shown but must also be included in calculations

decreasing rapidly with increasing  $Q^2$  as shown by the red data points in Fig. 1.

The most commonly proposed explanation for this discrepancy is “hard” two-photon exchange contributions beyond the standard radiative corrections to one-photon exchange [19]. Two-photon exchange, TPE, (see Fig. 2) is generally included as part of the radiative corrections when analyzing electron-proton scattering.

However, it is usually only included in the “soft” limit where one of the two photons, in the diagrams with two photons, is assumed to carry negligible momentum and the intermediate hadronic state remains a proton. To include “hard” two-photon exchange, a model for the off-shell, intermediate hadronic state must also be included, making the calculations difficult and model dependent.

Recent experiments, including the OLYMPUS experiment at DESY, show little evidence for significant contributions beyond single photon exchange up to  $Q^2 \approx 2.3 \text{ (GeV/c)}^2$ . To determine if “hard” two-photon exchange contributions can explain the form factor discrepancy new measurements at higher  $Q^2$  are necessary.

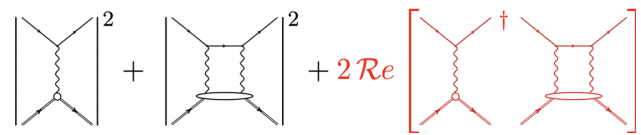


**Fig. 3** Square of the first two Feynman diagrams for one- and two-photon exchange

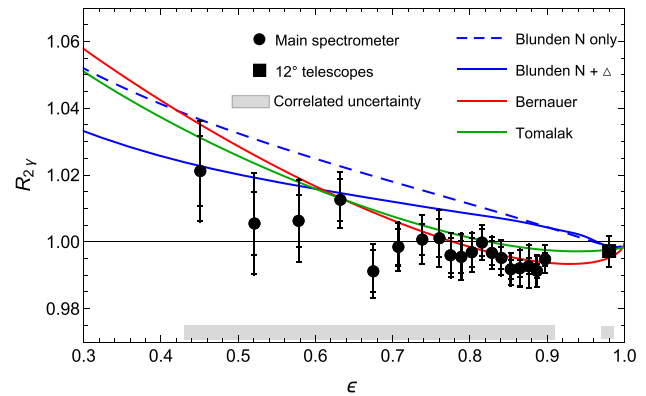


**Fig. 4** OLYMPUS results for  $R_{2\gamma}$  as a function of  $\epsilon$ . Inner error bars are statistical while the outer error bars include uncorrelated systematic uncertainties added in quadrature. The gray band represents the correlated systematic uncertainty

To measure the “hard” two-photon contribution, one can measure the ratio  $R_{2\gamma} = \sigma_{e+p}/\sigma_{e-p}$  at different values of  $Q^2$  and  $\epsilon$ . Following the Feynmann rules to calculate the cross sections,  $\sigma_{e\pm p}$ , one squares the matrix elements. Using just the first two diagrams shown in Fig. 2 as an illustrative example one gets:

Note the interference term between one- and two-photon exchange diagrams (shown in Fig. 3) has an odd number of lepton vertices. This means it will change sign between electron and positron scattering and can provide a measure of the two-photon exchange contribution.

The results from the OLYMPUS experiment [20] are shown in Fig. 4 together with various calculations.

The deviation of the results from unity are small, on the order of 1%, and are below unity at large  $\epsilon$  and rising with decreasing  $\epsilon$ . The dispersive calculations of Blunden [21] are systematically above the OLYMPUS results in this energy regime. The phenomenological prediction from Bernauer [22] and the subtractive dispersion calculation from Tomalak [23] are in better agreement with the OLYMPUS results but appear to rise too quickly as  $\epsilon$  decreases. There is some indication that TPE increases with decreasing  $\epsilon$  or increasing  $Q^2$ , suggesting that a significant “hard” two-photon contribution might be present at lower  $\epsilon$  or higher  $Q^2$ .

Two other experiments, VEPP-3 [24] and CLAS [25], also measured the “hard” two-photon exchange contribution to electron-proton elastic scattering.

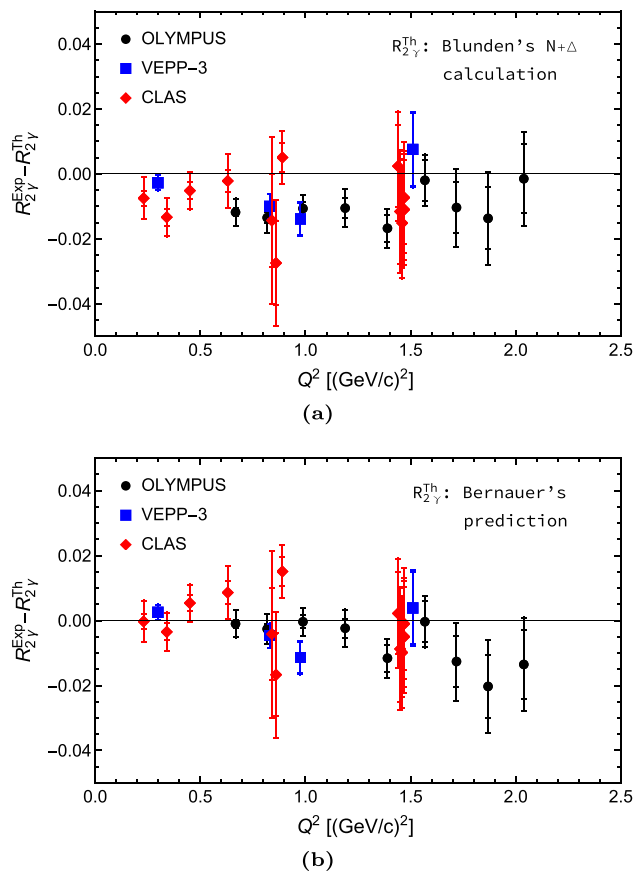


**Fig. 5** Difference between the results from the three recent experiments and **a** Blunden’s N+Δ calculation and **b** Bernauer’s prediction

It is difficult to compare the results from the three experiments directly since the measurements are at different points in the  $(\epsilon, Q^2)$  plane. To partially account for this, we can compare all the two-photon exchange results by taking the difference with respect to a selected calculation evaluated at the correct  $(\epsilon, Q^2)$  for each data point. This is shown in Fig. 5a for Blunden’s calculation and in Fig. 5b for Bernauer’s phenomenological prediction, plotted versus  $Q^2$ . In these views, the results from the three experiments are shown to be in reasonable agreement supporting the previous conclusions.

The results from the three TPE experiments are all below  $Q^2 = 2.3 \text{ (GeV/c)}^2$ . In this regime the discrepancy in the form factor ratios is not obvious, so the small “hard” TPE contribution measured is consistent with the measured form factor ratios. The increase in  $R_{2\gamma}$  with decreasing  $\epsilon$  in Fig. 4 suggests that TPE may be important at smaller  $\epsilon$  or higher  $Q^2$ . But, since this slope appears to deviate from Bernauer’s phenomenological prediction, which fits the observed discrepancy, it may also suggest that “hard” TPE, while contributing, may not explain all of the observed form factor discrepancy.

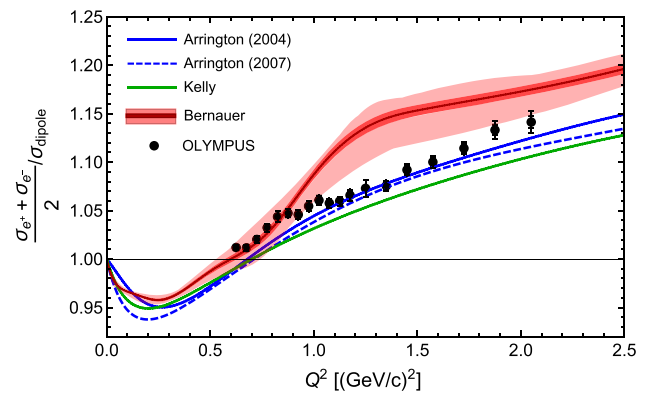


**Fig. 6** The charge-averaged yield for elastic lepton-proton scattering from the OLYMPUS experiment [26]

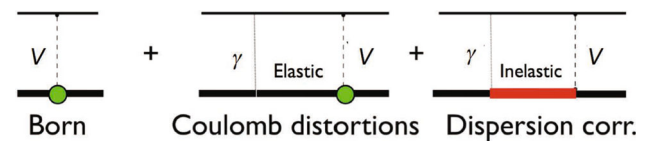


**Fig. 7** More general electroweak box diagram (where  $V = Z^0, W^\pm, \text{ or } \gamma$ ) that is important in many fundamental nuclear physics processes

Recently, the OLYMPUS data has also been analyzed to determine the charge-averaged yield for elastic lepton-proton scattering [26]. The result is shown in Fig. 6.

This measurement is insensitive to any charge-odd radiative corrections including “hard” two-photon exchange and thus provides a better measure of the proton form factors. The data shown covers an important range of  $Q^2$  where the  $G_M$  form factor changes slope. The calculations by Kelly [27] and Arrington [28,29] appear to be in better agreement with the data, but Bernauer’s global fit [22] should be redone to incorporate all the OLYMPUS data.

The two-photon exchange diagram in the QED expansion for electron scattering is an example of the more generic electroweak photon-boson diagram (see Fig. 7) which enters into a number of fundamental processes in subatomic physics. The  $\gamma - Z$  box is a significant contribution to the asymmetry in parity-violating electron scattering and the  $\gamma - W^\pm$  box is an important radiative correction in  $\beta$ -decay which must be implemented to extract  $V_{ud}$  of the Standard Model from  $0^+ \rightarrow 0^+$  super-allowed nuclear  $\beta$ -decays.

The proton form factors are fundamental to hadronic physics. Understanding the QED expansion, the role of two-photon exchange, and the scale of radiative corrections at higher  $Q^2$  will be crucial in future studies at FAIR, JLab, EIC, and elsewhere. The charge-averaged yield eliminates all charge-odd radiative corrections including the leading terms of two-photon exchange, which cannot be calculated with current theories. Measuring the ratio of positron-proton to electron-proton scattering is sensitive to the charge-odd

radiative corrections and insensitive to the charge-even radiative corrections. Together they help to study radiative corrections and unravel the proton form factors. TPEX, will provide access to both charge-odd and charge-even measurements at higher  $Q^2$ .

The discrepancy in the form factor ratio has not been resolved and the role played by two-photon exchange continues to be widely discussed within the nuclear physics community [19,30–33]. Further measurements and theoretical work on the role of two-photon exchange on the proton form factors are clearly needed. However, measurements at higher  $Q^2$  and smaller  $\epsilon$ , where the discrepancy is clear and TPE are expected to be larger, are difficult as the cross sections decrease rapidly. In addition, there are not many laboratories capable of providing both electron and positron beams with sufficient intensity.

The best, and for the foreseeable future only, opportunity is at DESY. This proposal outlines an experiment that could measure  $R_{2\gamma}$  at  $Q^2$  up to  $4.6 \text{ (GeV/c)}^2$  or higher, and  $\epsilon$  below 0.1 where the form factor discrepancy is clear (see Fig. 1). Such an experiment would overlap with the existing OLYMPUS data as a cross-check and would map out the two-photon exchange contribution over a broad range in  $Q^2$  and  $\epsilon$  to provide data to constrain theoretical calculations.

## 2 Proposed experiment

A schematic overview of the TPEX experimental setup is shown in Fig. 8. The electron or positron beam enters the vacuum chamber along the beamline (upper-right) and passes through the 20 cm long liquid hydrogen target (Sect. 2.1) before reaching the beamdump (Sect. 2.5).

At  $\pm 8^\circ$  there are 3 m long beampipes that connect the scattering chamber to the lead collimators before the Cherenkov detectors, used to monitor the luminosity (Sect. 2.4). These beampipes are under vacuum and reduce the multiple scattering for the relatively low energy (30–50 MeV) Møller and Bhabha scattered leptons. Ten scattered particle spectrometers are placed at polar angles of  $30^\circ$ ,  $50^\circ$ ,  $70^\circ$ ,  $90^\circ$ , and  $110^\circ$  to the left and right of the beam axis with the front face of the calorimeter modules at a radius of 1 m from the target. Each spectrometer consists of a  $5 \times 5$  array of lead tungstate crystals calorimeter (Sect. 2.2) and two planes of GEM detector (Sect. 2.3).

### 2.1 Liquid hydrogen target and scattering chamber

Figure 9 depicts the conceptual design of the liquid hydrogen target system. Figure 9a provides a schematic overview of the target system, which consists of the scattering chamber, the cryo-cooler system, and the 20 cm long, and 2 cm wide target cell. The dimensions of the scattering chamber windows are

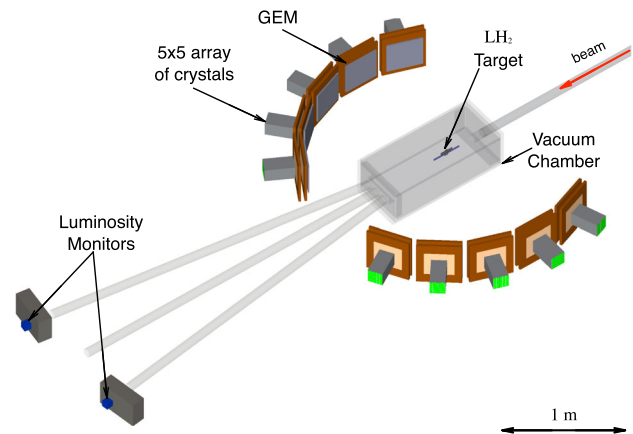


**Fig. 8** Schematic layout of a proposed TPEX target, scattering chamber, and detector configuration including the luminosity monitors and beamlines. The lepton beam would enter through the beamline in the upper-right, traverse the target cell, and scatter into the detectors or continue straight to the beamdump

determined from the solid angle subtended by the calorimeters. The two side exit windows cover the polar angles for the lead tungstate calorimeters in the range of  $25^\circ < \theta < 120^\circ$ . At the end of the 3 m long beam pipes leading to the luminosity monitors are two small exit windows cover a range of  $7^\circ < \theta < 9^\circ$ . The vertical dimensions of the two side exit windows cover an azimuthal angle of  $\phi = 0^\circ \pm 10^\circ$ . To maximize rigidity and withstand the enormous force from atmospheric pressure, as well as to avoid welded and bolted joints, we propose to machine the scattering chamber from a single piece of aluminum.

Details of the liquid hydrogen target system are shown in Fig. 9b. The cryo-cooler/condenser combination will closely follow the successful MUSE design [34]. We will therefore use the CH110-LT single-stage cryo-cooler from Sumitomo Heavy Industries Ltd [35] for refrigeration. This cryo-cooler has a cooling power of 25 W at 20 K, which is more than sufficient to cool down and fill the 70 ml  $\text{LH}_2$  target cell in approximately 2 h [34].

### 2.2 Lead tungstate calorimeters

For the proposed experiment, we are capitalizing on the R&D experience [36,37] gained from the CMS experiment and its subsequent applications by the Bonn and Mainz groups at CEBAF [38] and for PANDA [39]. We plan to utilize ten  $5 \times 5$  arrays of lead tungstate ( $\text{PbWO}_4$ ) crystals, totaling 250 crystals. By employing the central  $3 \times 3$  array of crystals within each  $5 \times 5$  array to define the acceptance, we achieve a solid angle of 3.6 msr at each angle. With a 20 cm long liquid hydrogen target, the acceptance range spans  $\pm 5.7^\circ$  in both polar and azimuthal angles. Consequently, the data obtained will be averaged over a small range in  $Q^2$  and  $\epsilon$ .

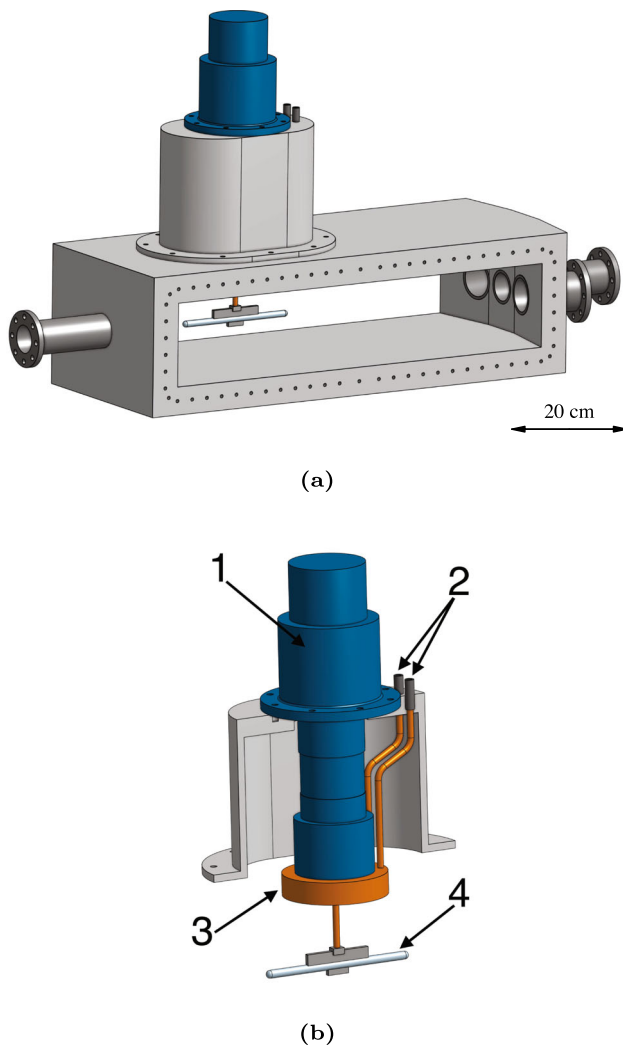


**Fig. 9** Conceptual design of the TPEX target chamber: **a** shows the full chamber view with the lepton beam entering from the left; **b** is a sectional drawing of the cryocooler system (1 – CH110-LT cryocooler, 2 – hydrogen supply and exhaust lines, 3 – condenser with a cooling loop, 4 – target cell)

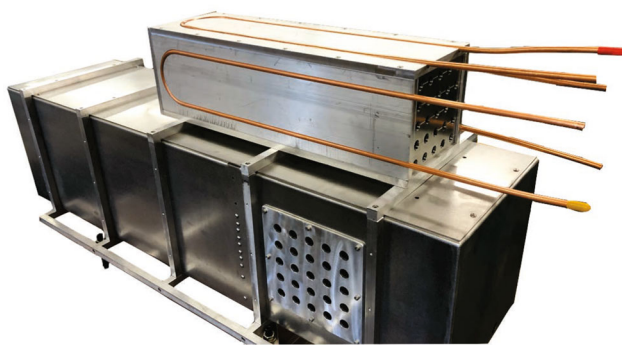


**Fig. 10** The prototype of the  $5 \times 5$  array of lead tungstate crystals calorimeter tested at DESY

We plan to use crystals with dimensions of  $2 \times 2 \times 20 \text{ cm}^3$ . With a density of  $8.3 \text{ g}\cdot\text{cm}^{-3}$ , each crystal weighs approximately 664 g, resulting in a total weight of 16.6 kg for a  $5 \times 5$  array of crystals. Lead tungstate has a radiation length  $X_0 = 0.8904 \text{ cm}$ , so these crystals are approximately  $22.5 X_0$  for good longitudinal electromagnetic shower confinement. The Molière radius is 1.959 cm, so using just the central  $3 \times 3$  array of crystals for acceptance, the outer ring of crystals contains the transverse shower adequately. Considering the nuclear interaction length of lead tungstate, which is  $\lambda_I = 20.28 \text{ cm}$ , the crystals are roughly  $0.986 \lambda_I$ . For the lepton energy range of interest, the energy resolution achieved with lead tungstate is approximately 2%.

The initial tests of the lead tungstate crystals calorimeter prototype (Fig. 10) at DESY have demonstrated reliable performance and a reconstructed energy resolution that is compatible with the requirements of TPEX. Detailed information regarding these tests can be found in Refs. [40,41].

### 2.3 GEM detectors

In addition to the lead tungstate crystals calorimeter, each scattered particle spectrometer is equipped with two planes of Gas Electron Multiplier (GEM) with two-dimensional read-out. Thin absorbers will be placed between the target and the GEMs to stop low-energy Møller or Bhabha leptons.

The GEMs provide spatial information of the traversing charged particle at the 100 micrometer precision level. By combining the hits on two GEM planes, a track segment is formed, providing directional information from the impact point on the calorimeter back to the event origin in the target. This serves to effectively suppress charged-particle backgrounds originating from regions other than the target. Furthermore, the GEM detectors are insensitive to neutral particles, making them effective in providing a veto against photons and neutrons. Additionally, by incorporating the calorimeter hit as a third tracking point, the efficiency of each component can be measured.

An active area of slightly more than  $20 \times 20 \text{ cm}^2$  is required to fully cover the area of the calorimeter entrance. A total of 20 elements is required to instrument ten calorimeter arms.

### 2.4 Luminosity and beam alignment monitor

The relative luminosity between the electron and positron running modes is the crucial normalization for the proposed measurement. The luminosity could be monitored by a pair of small-angle detectors positioned downstream on either side of the beamline. This approach was also used in the OLYMPUS experiment [42], and based on the lessons learned from that experiment, could be improved substantially. Given the running conditions of the proposed measurement, we favor a pair of quartz Cherenkov counters positioned  $8^\circ$  from the

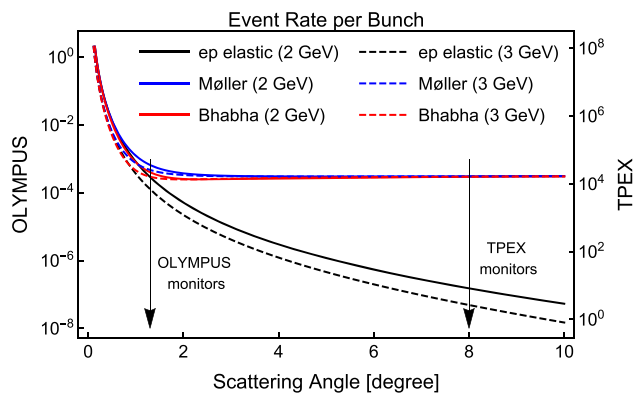


**Fig. 11** Whereas the forward monitors in OLYMPUS had an event per bunch rate well below 1, the TPEX monitors will see  $10^4$  Møller or Bhabha events per bunch crossing

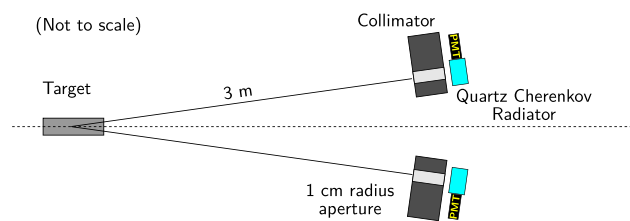


**Fig. 12** Schematic for the proposed luminosity monitor, consisting of two quartz Cherenkov detectors with an acceptance defined by 1 cm radius apertures in high-Z collimators

beamline to monitor the rates of Møller and Bhabha scattering from atomic electrons in the target.

A monitor placed at  $8^\circ$  has a number of advantages relative to the  $1.3^\circ$  placement of the OLYMPUS luminosity monitors. First, at  $8^\circ$ , the Møller and Bhabha cross sections are only a few percent different, whereas for the OLYMPUS monitors, which covered the symmetric angle ( $90^\circ$  in the center-of-mass frame), the two cross sections differed by over 50%, with significant angular dependence. Second, the Møller/Bhabha rate completely dwarfs the  $e^\pm p$  elastic scattering rate, meaning that it is really only sensitive to QED processes. No form factors or any other hadronic corrections<sup>1</sup> are needed to calculate the Møller and Bhabha cross sections. Third, the sensitivity to alignment scales as  $1/\sin\theta$ , meaning the monitor will be much more robust to small misalignments, which were a significant challenge for the OLYMPUS luminosity monitor.

A schematic layout of the design is shown in Fig. 12. The monitor consists of two quartz Cherenkov detectors, which act as independent monitors. Cherenkov detectors were chosen because they are widely used for monitoring in high-rate applications, such as in parity-violating electron scattering [43,44]. The two detectors operate independently and can

<sup>1</sup> Other than the radiative correction from vacuum polarization.

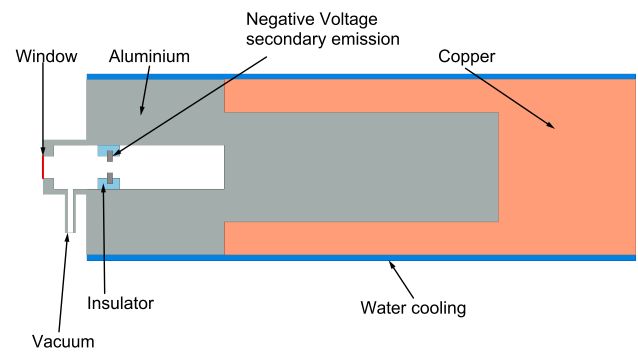


**Fig. 13** Schematic view of a possible beamdump/Faraday cup for TPEX

cross-check each other, helping to reduce systematic errors from beam alignment.

### 2.5 Beamdump/Faraday cup

A new extracted beam facility from DESY II will need a beamdump. Figure 13 shows the conceptual design of the beamdump for TPEX experiment. Assuming a maximum current of 100 nA and a beam energy of 7 GeV the maximum power to be handled is 700 W. To contain the showering, the beamdump used to have order of 5 Molière radii laterally and order of 25 radiation lengths longitudinally.

To augment the luminosity measurement proposed in Sect. 2.4 it is considered to modify the beamdump to also function as a Faraday cup to integrate the charge that passes through the target. Then, assuming the length of the target cell and density of liquid hydrogen are known, a measure of the luminosity can be obtained online. As shown in Fig. 13, an insulated ring held at negative voltage of a few hundred volts is needed to suppress secondary emission from back scattering out of the Faraday cup.

## 3 Plans and expectations

We propose to commission the experiment using 2 GeV electrons. We do this to commission the electronics, detectors, and data acquisition system taking advantage of the relatively high cross section at 2 GeV. About 2 weeks of beam time is required for this commissioning after the experiment was installed and surveyed. We would also like a brief run (few days) with positrons to verify that the beam alignment and performance do not change with positron running. The commissioning run (including a few days with positrons) would also allow a crosscheck of the OLYMPUS data at  $30^\circ$ ,  $50^\circ$ , and  $70^\circ$  and give a modest extension in  $Q^2$  up to  $2.7 (\text{GeV}/c)^2$ .

Table 1 shows  $Q^2$ ,  $\epsilon$ , differential cross section, and event rate expected for one day of running for the proposed

**Table 1** Kinematics, cross section, and events expected in one day for an incident lepton beam of 2 GeV and 40 nA averaged current on a 20cm liquid hydrogen target

$\theta$	$Q^2$ (GeV/c) <sup>2</sup>	$\epsilon$	$d\sigma/d\Omega$ fb	Events/day
30°	0.834	0.849	$2.41 \times 10^7$	$3.16 \times 10^6$
50°	1.62	0.611	$7.66 \times 10^5$	$1.01 \times 10^5$
70°	2.19	0.386	$1.00 \times 10^5$	$1.32 \times 10^4$
90°	2.55	0.224	$2.81 \times 10^4$	$3.70 \times 10^3$
110°	2.78	0.120	$1.22 \times 10^4$	$1.61 \times 10^3$

**Table 2** Kinematics, cross section, and events expected in one day for an incident lepton beam of 3 GeV and 40 nA averaged current on a 20cm liquid hydrogen target and 3.6 msr acceptance and a left/right symmetric detector configuration

$\theta$	$Q^2$ (GeV/c) <sup>2</sup>	$\epsilon$	$d\sigma/d\Omega$ fb	Events/day
30°	1.69	0.825	$2.41 \times 10^6$	$3.16 \times 10^5$
50°	3.00	0.554	$6.51 \times 10^4$	$8.55 \times 10^3$
70°	3.82	0.329	$8.94 \times 10^3$	$1.17 \times 10^3$
90°	4.29	0.184	$2.65 \times 10^3$	$3.48 \times 10^2$
110°	4.57	0.096	$1.20 \times 10^3$	$1.58 \times 10^2$

left/right symmetric configuration with 2 GeV lepton beams averaging 40 nA on a 20 cm liquid hydrogen target and using just the central 3 × 3 array of crystals to calculate the acceptance area.

The main TPEX run would be made at 3.0 GeV and would require approximately 6 weeks (2 weeks with electrons and 4 weeks with positrons in total) to collect the required data. Table 2 shows  $Q^2$ ,  $\epsilon$ , differential cross section, and event rate expected for one day of running for the proposed configuration with 3 GeV lepton beams. This would extend the measurements to  $Q^2 = 4.57$  (GeV/c)<sup>2</sup> where the form factor ratio discrepancy is large. The 6 weeks could be divided into shorter periods if that fit better with the DESY synchrotron schedule though longer, uninterrupted runs would be preferable. To minimize systematics we would like to switch between positron and electron running as frequently as possible (e.g. 1 day positron, 1 day electron, and 1 day positron repeating).

The  $Q^2$  range that the proposed TPEX experiment would be capable of reaching is shown in Fig. 14 for the 2 and 3 GeV runs of this proposal. The reach with TPEX can be seen in relation to the discrepancy in the form factor ratio. With additional crystals at back angles the 4 GeV runs would also be possible in a reasonable time frame.

The TPEX experiment at DESY would also measure the charge-averaged cross section just like the recent result from OLYMPUS (see Fig. 6). As mentioned above this cross sec-

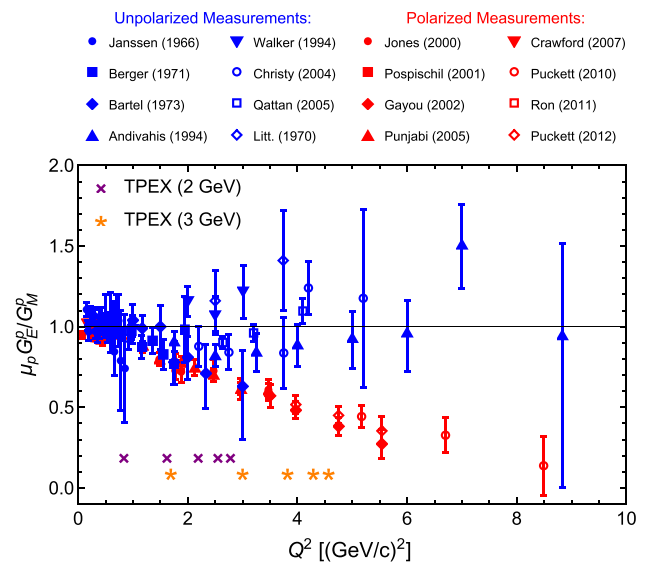


**Fig. 14** Proton form factor ratio as before but also showing the  $Q^2$  range accessible with the proposed TPEX configuration at 2 and 3 GeV. The 4 GeV range would be possible with additional crystals

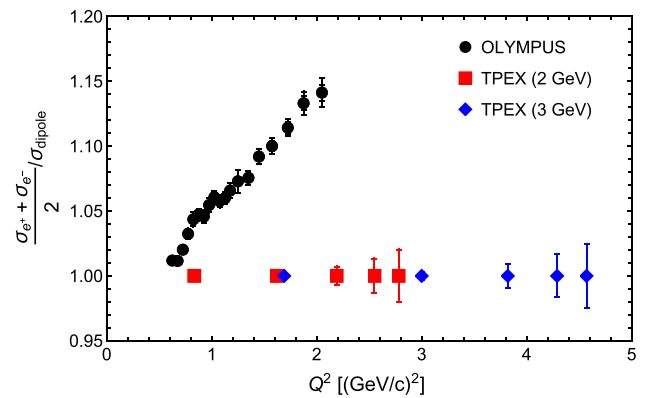


**Fig. 15** Charge-averaged cross section divided by the dipole cross section from OLYMPUS and expected uncertainties and coverage from TPEX at 2 and 3 GeV

tion is insensitive to charge-odd radiative corrections including “hard” two-photon exchange terms. Thus, it provides a more robust measure of the proton form factors. The expected charge-averaged cross section uncertainties (assuming dipole cross section) are shown in Fig. 15 for TPEX assuming 6 days of running at 2 GeV and 6 weeks of running at 3 GeV with only 50% data collection efficiency. The recent OLYMPUS results are also shown.

### 4 Conclusion

The observed discrepancy in the proton form factor ratio presents a fundamental challenge in nuclear physics and quantum electrodynamics (QED). Despite the inclusion of leading order QED radiative corrections, these corrections



alone have proven insufficient to resolve the discrepancy. This suggests that higher order corrections might be necessary to achieve a comprehensive understanding of the phenomenon. Additionally, it is plausible that more detailed models for the intermediate hadronic state could be required to accurately account for the observed deviation. Furthermore, it is crucial to consider the possibility of alternative processes that may contribute to the observed discrepancy.

To address this issue and gain further insights into the proton form factors at higher momentum transfers, the establishment of an extracted positron and electron beam facility at Deutsches Elektronen-Synchrotron (DESY) would offer a unique opportunity. Such a facility would enable the measurement of the two-photon exchange contribution to elastic lepton-proton scattering across a kinematic range where the evident discrepancy is prominent. The proposed TPEX experiment outlines an initial plan for an experimental configuration that could help resolve this issue and provide insight to the radiative corrections needed to understand the proton form factors at higher momentum transfers.

**Acknowledgements** The measurements leading to these results have been performed at the Test Beam Facility [45] at DESY Hamburg (Germany), a member of the Helmholtz Association (HGF). This work was supported by the US National Science Foundation (NSF) Grants PHY-2012114, PHY-1812402, PHY-2113436, PHY2012430, PHY2309976, and PHY-2110229, by the US Department of Energy Office of Science, Office of Nuclear Physics, under Grants DE-SC0016583, DE-FG02-94ER40818, and DE-SC0013941. We also received support from the PIER Hamburg-MIT/BOS Seed Project PHM-2019-04 and MEYS of Czech Republic under grant LM2023034.

**Funding** Open Access funding provided by the MIT Libraries.

**Data Availability Statement** Data will be made available on reasonable request. [Author's comment: The data supporting the findings of this article are available within the article. Should further information be desired, we are pleased to accommodate any reasonable requests promptly.]

**Open Access** This article is licensed under a Creative Commons Attribution 4.0 International License, which permits use, sharing, adaptation, distribution and reproduction in any medium or format, as long as you give appropriate credit to the original author(s) and the source, provide a link to the Creative Commons licence, and indicate if changes were made. The images or other third party material in this article are included in the article's Creative Commons licence, unless indicated otherwise in a credit line to the material. If material is not included in the article's Creative Commons licence and your intended use is not permitted by statutory regulation or exceeds the permitted use, you will need to obtain permission directly from the copyright holder. To view a copy of this licence, visit <http://creativecommons.org/licenses/by/4.0/>.

## References

1. L.W. Mo, Y.S. Tsai, Radiative corrections to elastic and inelastic ep and  $\mu p$  scattering. *Rev. Mod. Phys.* **41**, 205–235 (1969). <https://doi.org/10.1103/RevModPhys.41.205>
2. L.C. Maximon, J.A. Tjon, Radiative corrections to electron-proton scattering. *Phys. Rev. C* **62**, 054320 (2000). <https://doi.org/10.1103/PhysRevC.62.054320>
3. T. Janssens, R. Hofstadter, E.B. Hughes, M.R. Yearian, Proton form factors from elastic electron-proton scattering. *Phys. Rev.* **142**, 922–931 (1966). <https://doi.org/10.1103/PhysRev.142.922>
4. C. Berger, V. Burkert, G. Knop, B. Langenbeck, K. Rith, Electromagnetic form-factors of the proton at squared four momentum transfers between  $10 \text{ fm}^{-2}$  and  $50 \text{ fm}^{-2}$ . *Phys. Lett.* **35B**, 87–89 (1971). [https://doi.org/10.1016/0370-2693\(71\)90448-5](https://doi.org/10.1016/0370-2693(71)90448-5)
5. J. Litt, Measurement of the ratio of the proton  $G(E)/G(M)$  form-factors at high momentum transfer and question of scaling. *Phys. Lett.* **31B**, 40–44 (1970). [https://doi.org/10.1016/0370-2693\(70\)90015-8](https://doi.org/10.1016/0370-2693(70)90015-8)
6. W. Bartel, F.W. Busser, W.R. Dix, R. Felst, D. Harms, H. Krehbiel, P.E. Kuhlmann, J. McElroy, J. Meyer, G. Weber, Measurement of proton and neutron electromagnetic form-factors at squared four momentum transfers up to  $3\text{-GeV}/c^2$ . *Nucl. Phys. B* **58**, 429–475 (1973). [https://doi.org/10.1016/0550-3213\(73\)90594-4](https://doi.org/10.1016/0550-3213(73)90594-4)
7. L. Andivahis, Measurements of the electric and magnetic form-factors of the proton from  $Q^2 = 1.75$  to  $8.83 \text{ (GeV}/c)^2$ . *Phys. Rev. D* **50**, 5491–5517 (1994). <https://doi.org/10.1103/PhysRevD.50.5491>
8. R.C. Walker, Measurements of the proton elastic form-factors for  $1 \leq Q^2 \leq 3 \text{ (GeV}/c)^2$  at SLAC. *Phys. Rev. D* **49**, 5671–5689 (1994). <https://doi.org/10.1103/PhysRevD.49.5671>
9. M. E. Christy, Measurements of electron proton elastic cross-sections for  $0.4 < Q^2 < 5.5 \text{ (GeV}/c)^2$ . *Phys. Rev. C* **70**, 015206 (2004). <https://doi.org/10.1103/PhysRevC.70.015206> [arXiv:nucl-ex/0401030](https://arxiv.org/abs/nucl-ex/0401030) [nucl-ex]
10. I.A. Qattan, Precision Rosenbluth measurement of the proton elastic form-factors. *Phys. Rev. Lett.* **94**, 142301 (2005). <https://doi.org/10.1103/PhysRevLett.94.142301> [arXiv:nucl-ex/0410010](https://arxiv.org/abs/nucl-ex/0410010) [nucl-ex]
11. M.K. Jones,  $G(E_p)/G(M_p)$  ratio by polarization transfer in  $ep \rightarrow ep$ . *Phys. Rev. Lett.* **84**, 1398–1402 (2000). <https://doi.org/10.1103/PhysRevLett.84.1398> [arXiv:nucl-ex/9910005](https://arxiv.org/abs/nucl-ex/9910005) [nucl-ex]
12. T. Pospischil, Measurement of  $G_{E_p}/G_{M_p}$  via polarization transfer at  $Q^2 = 0.4 \text{ (GeV}/c)^2$ . *Eur. Phys. J. A* **12**, 125–127 (2001). <https://doi.org/10.1007/s100500170046>
13. O. Gayou, Measurements of the elastic electromagnetic form-factor ratio  $\mu_p G_{E_p}/G_{M_p}$  via polarization transfer. *Phys. Rev. C* **64**, 038202 (2001). <https://doi.org/10.1103/PhysRevC.64.038202>
14. V. Punjabi, Proton elastic form-factor ratios to  $Q^2 = 3.5 \text{ GeV}^2$  by polarization transfer. *Phys. Rev. C* **71**, 055202 (2005) <https://doi.org/10.1103/PhysRevC.71.055202> [arXiv:nucl-ex/0501018](https://arxiv.org/abs/nucl-ex/0501018) [nucl-ex]. [Erratum: *Phys. Rev. C* **71**, 069902 (2005)]
15. C. Crawford, Measurement of the Proton's electric to magnetic form factor ratio from  $^1\text{H}(e, ep)$ . *Phys. Rev. Lett.* **98**(5), 052301 (2007)
16. A.J.R. Puckett, Recoil polarization measurements of the proton electromagnetic form factor ratio to  $Q^2 = 8.5 \text{ GeV}^2$ . *Phys. Rev. Lett.* **104**, 242301 (2010) <https://doi.org/10.1103/PhysRevLett.104.242301>, [arXiv:1005.3419](https://arxiv.org/abs/1005.3419) [nucl-ex]
17. G. Ron, Low  $Q^2$  measurements of the proton form factor ratio  $\mu_p G_E/G_M$ . *Phys. Rev. C* **84**, 055204 (2011). <https://doi.org/10.1103/PhysRevC.84.055204> [arXiv:1103.5784](https://arxiv.org/abs/1103.5784) [nucl-ex]
18. A.J.R. Puckett, Final analysis of proton form factor ratio data at  $Q^2 = 4.0, 4.8$  and  $5.6 \text{ GeV}^2$ . *Phys. Rev. C* **85**, 045203 (2012) <https://doi.org/10.1103/PhysRevC.85.045203>, [arXiv:1102.5737](https://arxiv.org/abs/1102.5737) [nucl-ex]
19. A. Afanasev, P.G. Blunden, D. Hasell, B.A. Raue, Two-photon exchange in elastic electron-proton scattering. *Prog. Part. Nucl. Phys.* **95**, 245–278 (2017) <https://doi.org/10.1016/j.pnpnp.2017.03.004>, [arXiv:1703.03874](https://arxiv.org/abs/1703.03874) [nucl-ex]

20. B.S. Henderson, Hard two-photon contribution to elastic lepton-proton scattering: determined by the OLYMPUS experiment. *Phys. Rev. Lett.* **118**(9), 092501 (2017). <https://doi.org/10.1103/PhysRevLett.118.092501>. arXiv:1611.04685 [nucl-ex]
21. P.G. Blunden, W. Melnitchouk, Dispersive approach to two-photon exchange in elastic electron-proton scattering. *Phys. Rev. C* **95**(6), 065209 (2017). <https://doi.org/10.1103/PhysRevC.95.065209>. arXiv:1703.06181 [nucl-th]
22. J.C. Bernauer, Electric and magnetic form factors of the proton. *Phys. Rev. C* **90**(1), 015206 (2014). <https://doi.org/10.1103/PhysRevC.90.015206>. arXiv:1307.6227 [nucl-ex]
23. O. Tomalak, M. Vanderhaeghen, Subtracted dispersion relation formalism for the two-photon exchange correction to elastic electron-proton scattering: comparison with data. *Eur. Phys. J. A* **51**(2), 24 (2015). <https://doi.org/10.1140/epja/i2015-15024-1>. arXiv:1408.5330 [hep-ph]
24. I.A. Rachek, Measurement of the two-photon exchange contribution to the elastic  $e^\pm p$  scattering cross sections at the VEPP-3 storage ring. *Phys. Rev. Lett.* **114**(6), 062005 (2015). <https://doi.org/10.1103/PhysRevLett.114.062005>. arXiv:1411.7372 [nucl-ex]
25. D. Adikaram, Towards a resolution of the proton form factor problem: new electron and positron scattering data. *Phys. Rev. Lett.* **114**, 062003 (2015). <https://doi.org/10.1103/PhysRevLett.114.062003>. arXiv:1411.6908 [nucl-ex]
26. J.C. Bernauer, et al., OLYMPUS: First measurement of the charge-averaged elastic lepton-proton scattering cross section (2020). arXiv:2008.05349 [nucl-ex]
27. J.J. Kelly, Simple parametrization of nucleon form factors. *Phys. Rev. C* **70**, 068202 (2004). <https://doi.org/10.1103/PhysRevC.70.068202>
28. J. Arrington, Evidence for two photon exchange contributions in electron proton and positron proton elastic scattering. *Phys. Rev. C* **69**, 032201 (2004). <https://doi.org/10.1103/PhysRevC.69.032201>. arXiv:nucl-ex/0311019
29. J. Arrington, W. Melnitchouk, J.A. Tjon, Global analysis of proton elastic form factor data with two-photon exchange corrections. *Phys. Rev. C* **76**, 035205 (2007). <https://doi.org/10.1103/PhysRevC.76.035205>. arXiv:0707.1861 [nucl-ex]
30. The Electroweak Box. (2017). <https://www.physics.umass.edu/acfi/seminars-and-workshops/the-electroweak-box>
31. S.K. Blau, Proton structure seen in a new light. *Phys. Today* **70**(5), 14–15 (2017). <https://doi.org/10.1063/PT.3.3541>
32. 2017, N.: The 11th International Workshop on the Physics of Excited Nucleons, Charlotte, SC. (2017). <http://nstar2017.physics.sc.edu/>
33. JPos 2017, JLab, Newport News, VA. (2017). <https://www.jlab.org/conferences/JPos2017/index.html>
34. P. Roy, A liquid hydrogen target for the MUSE experiment at PSI. *Nuclear Instrum. Methods Phys. Res. Sect. A* **949**, 162874 (2020). <https://doi.org/10.1016/j.nima.2019.162874>
35. Group, S.C.: CH-110 Series Cryocoolers System Configurations (2011). <http://www.shcryogenics.com/products/specialty-cryocoolers/ch-110lt-30k-cryocooler-series>
36. R.Y. Zhu, D.A. Ma, H.B. Newman, C.L. Woody, J.A. Kierstad, S.P. Stoll, P.W. Levy, A Study on the properties of lead tungstate crystals. *Nucl. Instrum. Method A* **376**, 319–334 (1996). [https://doi.org/10.1016/0168-9002\(96\)00286-0](https://doi.org/10.1016/0168-9002(96)00286-0)
37. R.Y. Zhu, Precision lead tungstate crystal calorimeter for CMS at LHC. *IEEE Trans. Nucl. Sci.* **51**, 1560–1567 (2004). <https://doi.org/10.1109/TNS.2004.832804>
38. D. Neyret, A Photon calorimeter using lead tungstate crystals for the CEBAF Hall A Compton polarimeter. *Nucl. Instrum. Meth. A* **443**, 231–237 (2000) [https://doi.org/10.1016/S0168-9002\(99\)01092-X](https://doi.org/10.1016/S0168-9002(99)01092-X), arXiv:hep-ex/9907047 [hep-ex]
39. M. Albrecht, The forward endcap of the electromagnetic calorimeter for the PANDA detector at FAIR. *J. Phys. Conf. Ser.* **587**(1), 012050 (2015). <https://doi.org/10.1088/1742-6596/587/1/012050>
40. I. Friščić, et al., Test of streaming and triggered readout schemes for the TPEX Lead Tungstate Calorimeter. *J. Instrument.* **18**(09), 09001 (2023). <https://doi.org/10.1088/1748-0221/18/09/P09001>
41. R. Alarcon, et al., Two-photon exchange – TPEX (2023). arXiv:2301.04708 [nucl-ex]
42. R. Préz Benito, Design and performance of a lead fluoride detector as a luminosity monitor. *Nucl. Instrum. Meth. A* **826**, 6–14 (2016). <https://doi.org/10.1016/j.nima.2016.04.071>, arXiv:1602.01702 [physics.ins-det]
43. S. Abrahamyan, Measurement of the neutron radius of  $^{208}\text{Pb}$  through parity-violation in electron scattering. *Phys. Rev. Lett.* **108**, 112502 (2012) <https://doi.org/10.1103/PhysRevLett.108.112502>, arXiv:1201.2568 [nucl-ex]
44. T. Allison, The  $Q_{weak}$  experimental apparatus. *Nucl. Instrum. Method. A* **781**, 105–133 (2015) <https://doi.org/10.1016/j.nima.2015.01.023>, arXiv:1409.7100 [physics.ins-det]
45. R. Diener, The DESY II test beam facility. *Nuclear Instrum. Methods Phys. Res. Sect. A* **922**, 265–286 (2019). <https://doi.org/10.1016/j.nima.2018.11.133>